www.sciencemag.org/cgi/content/full/science.aap9855/DC1

Supplementary Materials for

A radio counterpart to a neutron star merger

G. Hallinan,* A. Corsi, K. P. Mooley, K. Hotokezaka, E. Nakar, M. M. Kasliwal, D. L. Kaplan, D. A. Frail, S. T. Myers, T. Murphy, K. De, D. Dobie, J. R. Allison, K. W. Bannister, V. Bhalerao, P. Chandra, T. E. Clarke, S. Giacintucci, A. Y. Q. Ho, A. Horesh, N. E. Kassim, S. R. Kulkarni, E. Lenc, F. J. Lockman, C. Lynch, D. Nichols, S. Nissanke, N. Palliyaguru, W. M. Peters, T. Piran, J. Rana, E. M. Sadler, L. P. Singer

*Corresponding author. Email: gh@astro.caltech.edu

Published 16 October 2017 on *Science* First Release
DOI: 10.1126/science.aap9855

This PDF file includes:

1. Radio Data Reduction

1.1. VLA

Radio observations of the EM170817 field were carried out with the Karl G. Jansky Very Large Array (*36*) in its C, CnB, and B configurations, under our target of opportunity programs (VLA/16A-206; PI: A. Corsi; VLA/17A-374; PI: K. Mooley). All observations reported here were carried out in *C*-band (nominal center frequency of 6 GHz, with a bandwidth of 4 GHz and *S*-band (nominal center frequency of 3 GHz, with a bandwidth of 2 GHz) with the Wideband Interferometric Digital Architecture (WIDAR) correlator. We used QSO J1258-2219 (*C*-band) and QSO B1245-197 (*S*-band) as our phase calibrator sources, and 3C 286 or 3C 147 as flux and bandpass calibrators.

VLA data were calibrated and flagged for radio frequency interference (RFI) using the VLA automated calibration pipeline which runs in the Common Astronomy Software Applications package (CASA, *37*). When necessary, additional flags were applied manually after calibration. Images of the observed field were formed using the CLEAN algorithm (*38*), which we ran in the interactive mode. When deconvolving bright background sources, care was taken not to include any clean components near the emission of EM170817.

Observations carried out after 2017 September 1 UTC were intermittently affected by rapidly fluctuating phases (timescale ~ minutes) caused by the on-going enhanced solar activity and potentially related activity in the troposphere. To mitigate phase errors in the *S*-band, a single round of phase-only self-calibration (including all sources brighter than 50 μJy in the initial model) was performed. At *C*-band, uncorrected phase errors resulted in a lower amplitude for all sources in the field of EM170817 during the first week of September. We therefore calculated a correction factor to the measured flux densities of the radio transient by estimating the average fractional change in the flux density of unresolved background radio sources in the field for each affected epoch. These corrections amount to ~30% of the flux for the most affected epoch (UT 2017 September 5) and to ~17% of the flux on the date of first discovery in C-band (UT 2017 September 3). A revised strategy of rapid phase calibration was implemented for observations in both bands on and after UT 2017 September 7, which greatly reduced the impact of the solar activity.

The results of our VLA follow-up campaign of EM170817 are reported in Table S1. Flux measurement errors are calculated as the quadratic sum of the map root-mean-square (rms) noise plus a 5% fractional error on the measured flux which accounts for inaccuracies in the flux density calibration. Where necessary, an amplitude correction factor is applied for known phase error issues in *C* band data. For non-detections, upper-limits are calculated as the measured flux at the position of EM170817 plus 2× the map rms. An example map with a high signal-to-noise detection (11σ) of EM170817 is shown in Figure S1.

1.2. ATCA

We observed EM170817 on 2017 August 18, 21, 28 and September 05 using the Australia Telescope Compact Array (ATCA) under a target of opportunity program (CX391; PI: T. Murphy). During the Aug 18 observation the array was in the EW352 configuration, for all other observations it was in the 1.5A configuration. The Aug 18, 21 and 28 observations used two 2 GHz frequency bands with central frequencies of 8.5 and 10.5 GHz, while for the Sept 05 observation we centered these two frequency bands on 5.5 and 9.0 GHz. For all epochs, the flux scale and bandpass response was determined using the ATCA primary calibrator PKS B1934-638, and

observations of QSO B1245-197 were used to calibrate the complex gains. The visibility data were reduced using the standard routines in the MIRIAD environment (*39*). For the August 18 epoch we noted a systematic error in the flux calibration of QSO B1245-197 and therefore scaled the flux densities for this epoch using the values listed for QSO B1245-197 in the ATCA Calibrator Database V3.

The calibrated visibility data from the August observations were then inverted and cleaned using the MIRIAD tasks INVERT, CLEAN and RESTOR. For these observations, we modelled and removed the host galaxy, NGC 4993, using the CASA tool IMFIT to fit a single Gaussian to this source, constraining the center of the Gaussian to be at the prior known location of NGC 4993 with a size identical to the restoring beam. In the resulting residual image, we then used the CASA task IMSTAT to place 3σ limits on the emission of EM170817 by measuring the rms within a region with a size six times the restoring beam and centered on its location.

For our observation in September, the calibrated visibility data were then split into the separate bands (5.5 GHz and 9.0 GHz), averaged to 32 MHz channels, and imported into DIFMAP (*40*). Bright field sources were modeled separately for each band with a combination of point-source and Gaussian components with power-law spectra. Care was taken not to include any components near the emission of EM170817 to avoid false detection. The residual images from each band were then averaged to form a wide-band image centered at 7.25 GHz. Restored images for each band were also generated by convolving the model components with the restoring beam and then averaged to form a wide-band image. Using a fit region, with size equal to the resolving beam and centered on the known location of EM170817, we measure a 4.1σ radio peak of 25 +/-6 μJy in this wide-band image.

1.3. GMRT

We carried out observations of the EM170817 field with the Giant Metrewave Radio Telescope (GMRT) at 400 MHz, 700 MHz and 1.2 GHz under the Director's Discretionary Time (DDT) program (DDTB284; PI: K. De). Our first observation at 610 MHz was carried out with the GMRT Software Backend (GSB; *41*), with 32 MHz bandwidth. These data were calibrated, RFI flagged and imaged using the SPAM pipeline (*42*). All other observations, centered at 400 MHz (200 MHz bandwidth), 700 MHz and 1200 MHz (400 MHz bandwidth for both) were carried out using the upgraded GMRT Wideband Backend (GWB; *43*) to obtain the highest available sensitivities. For all observations, the pointing was centered at the location of the optical transient, 3C 283 was used as the complex gain calibrator and 3C 286 as the absolute flux scale and bandpass calibrators. These data were calibrated and RFI flagged using a custom-developed CASA pipeline. The data were then imaged interactively with the CASA task CLEAN, while incorporating a few iterations of phase-only self-calibration.

1.4. VLITE

The VLA Low Band Ionosphere and Transient Experiment (VLITE; *44*) is a parallel observing system on the VLA that records the 340-384 MHz data from the prime focus P band receivers for nearly all observing programs. We report here VLITE results associated with the VLA target of opportunity programs described above. VLITE data are processed through a custom calibration and imaging pipeline which incorporates algorithms from the AIPS (*45*) and Obit (*46*) data reduction packages. The pipeline runs daily and initially sorts all data by the primary VLA Cassegrain primary observing band. For each data set, it then uses standard tasks to perform two cycles of automated excision of RFI, delay calibration, bandpass correction, and flux calibration.

All primary calibration uses a set of seven frequently observed standard calibrators, which may be observed at that primary observing band at any time during the day. Following the calibration, the pipeline performs wide-field, wide-bandwidth imaging of each target with up to two rounds of phase-only self-calibration and one round of amplitude and phase self-calibration.

The data were processed through the standard VLITE pipeline. The self-calibrated data were then re-imaged by hand using the Obit task 'MFImage'. An RFI-free band of 34 MHz centered at 338.7 MHz was chosen, and only baselines longer than 0.5 kλ were included, where λ is the observation wavelength. An additional phase-only self-calibration followed by an amplitude and phase self-calibration were performed. When needed, the nearby bright source (3C 283) was calibrated separately in amplitude and phase, and subtracted from the data (peeled) to reduce artifacts from the source. On 25 Aug. some of the observations in our 17A-374 program did not directly target the source but fall within the large VLITE field of view in eight separate images from that program. We convolved those eight images to a common beam and combined them using Obit mosaic utility tasks and a primary beam model derived from VLITE archival data. For days when multiple observations of the target were made at different primary observing bands, the visibility data were combined and imaged jointly.

1.5. GBT

NGC 4933 was observed in the 21-cm line of neutral hydrogen on 2017 September 11 using the 100 m Robert C. Byrd Green Bank Telescope (GBT), under proposal GBT17B_395 (PI: F. Lockman) at an angular resolution of 9.1 arcminutes. Spectra were taken using the standard GBT L-band receiver (*47*) while the telescope was switched between the position of the galaxy and a nearby reference position for about 1 hour. The system was checked using observations of a known galaxy. A third order polynomial was fit to the final spectrum to remove a residual instrumental baseline. No 21-cm emission was detected at or near the expected velocity of 2900 km s^{-1} *(48)* (see Figure S2) to an rms noise level of 7.0 mK (3.5 mJy) in a channel of 1.51 km s^{-1}. We translate that into an approximate limit on the neutral hydrogen mass of NGC 4993 by assuming a velocity width of 200 km s^{-1}, finding a 5σ mass limit of $<1 \times 10^8$ $M_\odot$.

2. Afterglow Modeling

The radio light curves were calculated using a numerical code described in (*49*). The output light curves have been found to be largely consistent with light curves produced by the BOXFIT code (*50*). In short, our code approximates the jetted blast wave at any lab time as a single zone emitting region which is a part of a sphere with an opening angle, θ_i. The hydrodynamics, including the shock location and velocity and the jet spreading, are described in detail in (*51*). The hydrodynamic variables in the emitting region are taken as those that are immediately behind the shock. The emission from each location along the shock is calculated using standard afterglow theory (*25*), where the microphysics is parameterized by the fraction of internal energy that goes to the electrons, ε_e, the fraction of internal energy that goes to the magnetic field, ε_B, and the power-law index of the electron distribution, p. In all the models we used $\varepsilon_e = 0.1$ and $\varepsilon_B = 0.01$. In models that are consistent with the radio observations we used $p = 2.1$, so the models are also roughly consistent with the X-ray observations (*11,30*). In models that are inconsistent with the available radio observations we used the more typical value of $p = 2.4$. The code calculates the rest frame emissivity at any time and any location along the shock and the specific flux observed at any given viewing angle at any given time and frequency is then found by integrating the contribution over

equal-arrival-time surfaces, with a proper boost to the observer frame and taking into account the light travel time.

Supplementary Text

3. Independent Constraints on the Environment of GW170817

We can attempt to infer the local ISM environment of the merger from observational results on the global or local ISM for NGC 4993. However, the low star formation rate (SFR) of NGC 4993 and the lack of direct measures of the ISM at the position of EM170817 make this problematic (*5)*. Considering our upper limit on the mass of neutral hydrogen, M_{HI} of $< 1 \times 10^8$ $M_\odot$, as well as previous constraints (*52*), and assuming that the hydrogen is distributed uniformly over twice the stellar extent of the galaxy (estimated to be 18 × 16 kpc) implies a surface density of < 0.1 $M_\odot/pc^2$. Translating that into a local number density gives $n_{H\,I} < 0.04$ cm^{-3}, with the total number density at most a factor of a few higher (assuming a face-on disk with scale-height of 100 pc; if the distribution is more spherical then it will lead to a lower limit). Repeating this exercise with a Sersic H I distribution gives a similar limit. We can invert this exercise, and look at the implied H I surface density from the estimated SFR. If the SFR is $\sim 10^{-2}$ $M_\odot$/yr (*5*) and assuming the same stellar extent as above, we can translate that into a star formation rate density and use the Kennicutt-Schmidt law (*53*, with n=1.4) to estimate $M_{H\,I} \sim 10^7$ $M_\odot$, a factor of 10 lower than above. This would imply $n_{H\,I} \sim 0.004$ cm^{-3}.

4. Comparison of 6 GHz Data with Models

The data obtained at 6 GHz, particularly before September 7, is subject to larger errors associated with rapidly fluctuating phases than data collected at 3 GHz. This is primarily because there is insufficient flux present in the EM170817 field at 6 GHz for robust self-calibration. However, it is still instructive to compare the observed light curve with the models (Figure S3). With the exception of one outlier point, the data are consistent with either a cocoon or an off-axis jet. The measured flux density on September 03 lies substantially above the predicted flux from the models. This observation was taken at a very low elevation (15 – 25°) resulting in sidelobe flux from the host galaxy AGN contaminating the location of the radio source. This may account for the higher flux density in this epoch, although intrinsic variability or scintillation cannot be ruled out.

Combining data at 3 and 6 GHz, we can also place constraints on the spectral slope of the radio emission. Using data taken on September 7 at 6 GHz and September 8 at 3 GHz, i.e., 1 day apart, we construct a 2-point spectral energy distribution (SED) for the radio counterpart to EM170817. Figure S3 compares this 2-point SED with the predicted SED for each of the models at 22 days post-merger. The radio data are consistent with the model predictions of an optically thin spectrum between 3 and 6 GHz.

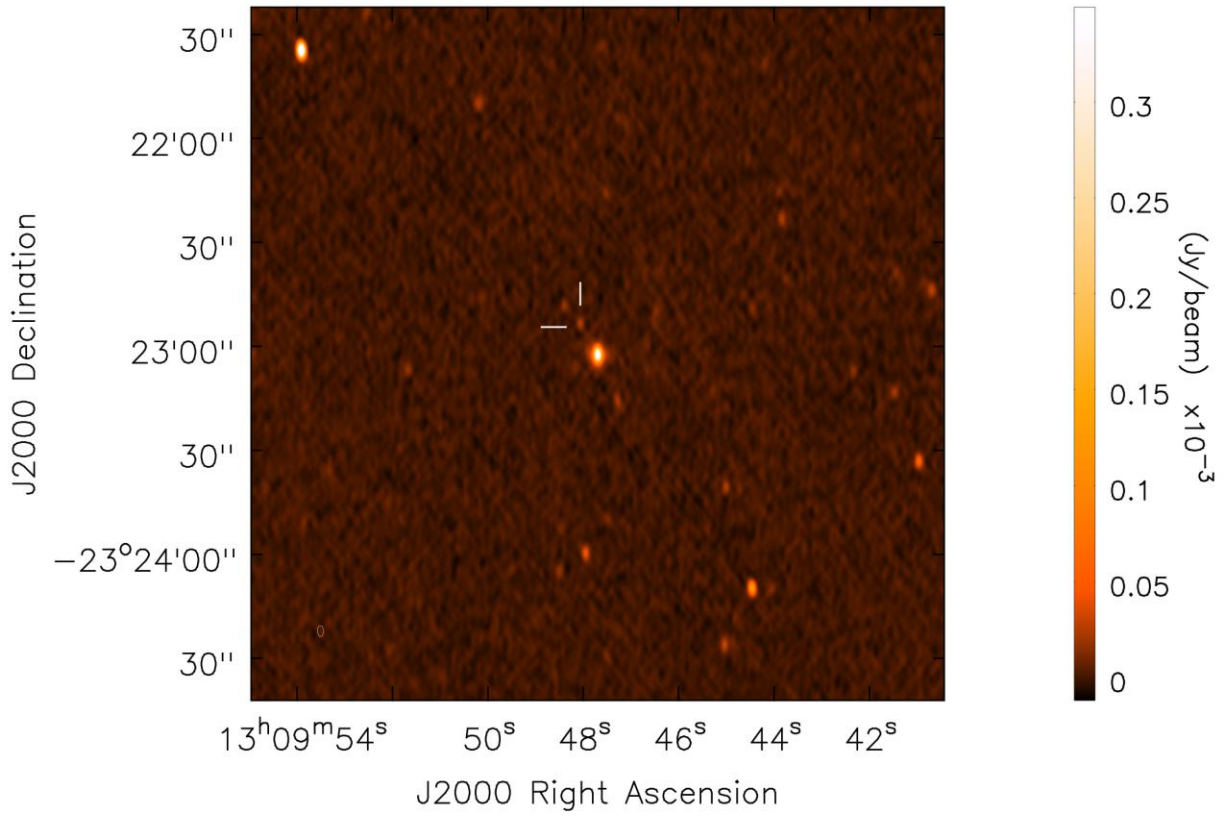

Fig. S1. Deep radio image of EM170817. A deep image of the ~3x3 arcminute field surrounding the location of NGC 4993 using VLA data at 3 GHz from 2017, September 8 and September 10. The AGN hosted by the galaxy is at the center of the image. The radio counterpart to EM170817 is highlighted and is detected at 25 +/- 2.2 μJy (11σ).

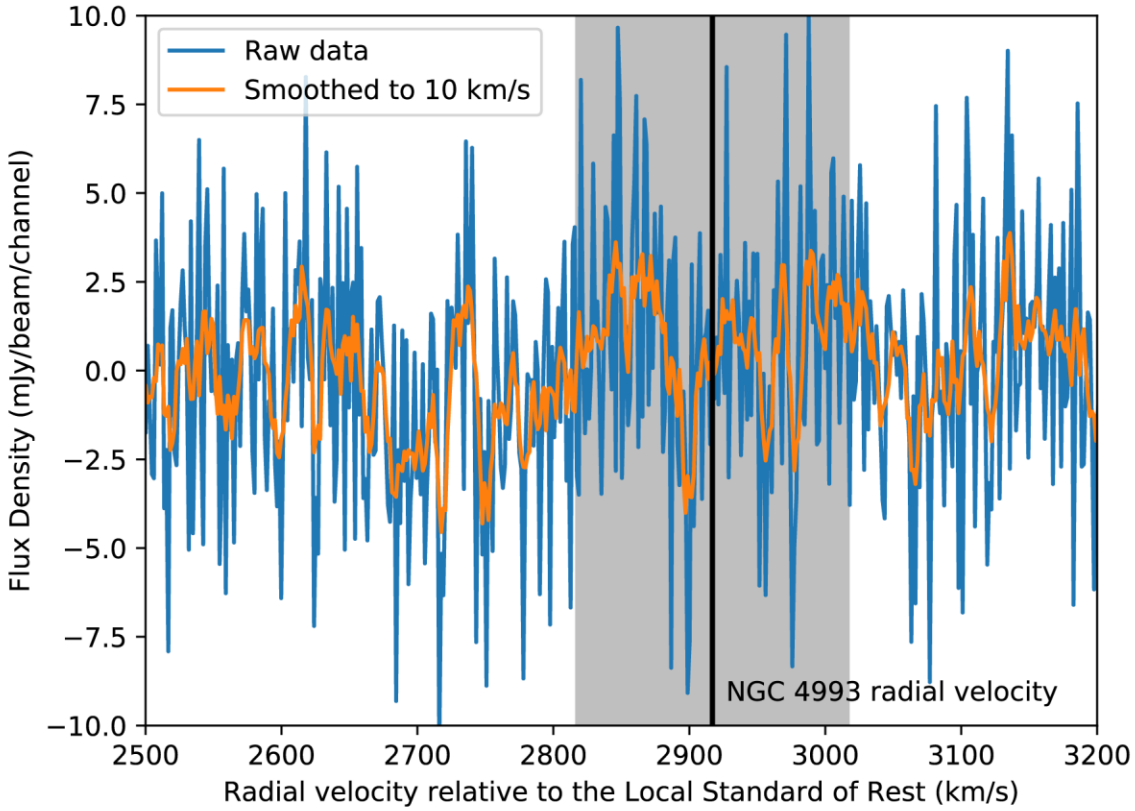

Fig. S2. Green Bank Telescope spectrum of neutral hydrogen in the 21 cm line toward NGC 4993. We plot the raw data in 1.5 km s^{-1} channels, as well as a version smoothed to 10 km s^{-1} channels, against radial velocity relative to the Local Standard of Rest. The radial velocity of NGC 4993 (*33*) is indicated with the vertical line, and the grey region spans a +/- 100 km s^{-1} velocity width that we used to estimate an upper limit on the neutral hydrogen mass.

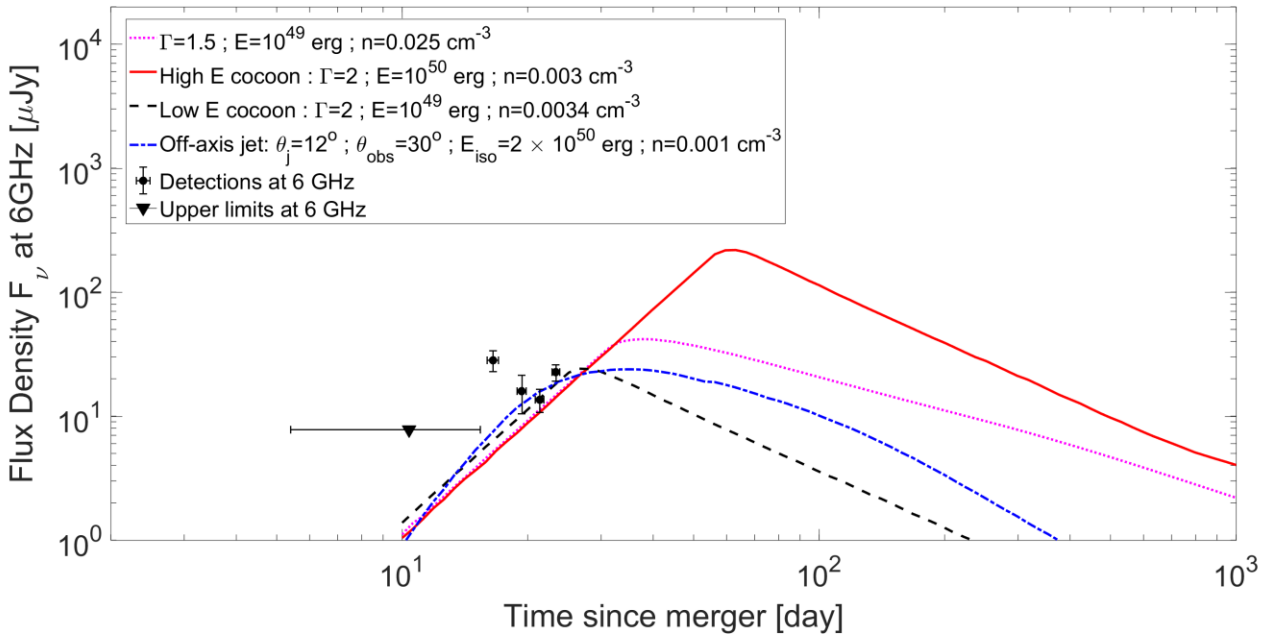

Fig. S3. Radio Light Curve at 6 GHz. We compare the light curve at 6 GHz with predictions from the four models previously shown in Fig. 3. With the exception of one outlier point, the data are consistent with either a cocoon or an off-axis jet. The flux density measurement on September 3 (16.5 days post-merger) was taken at very low elevation and is affected by sidelobe contamination from the host galaxy AGN.

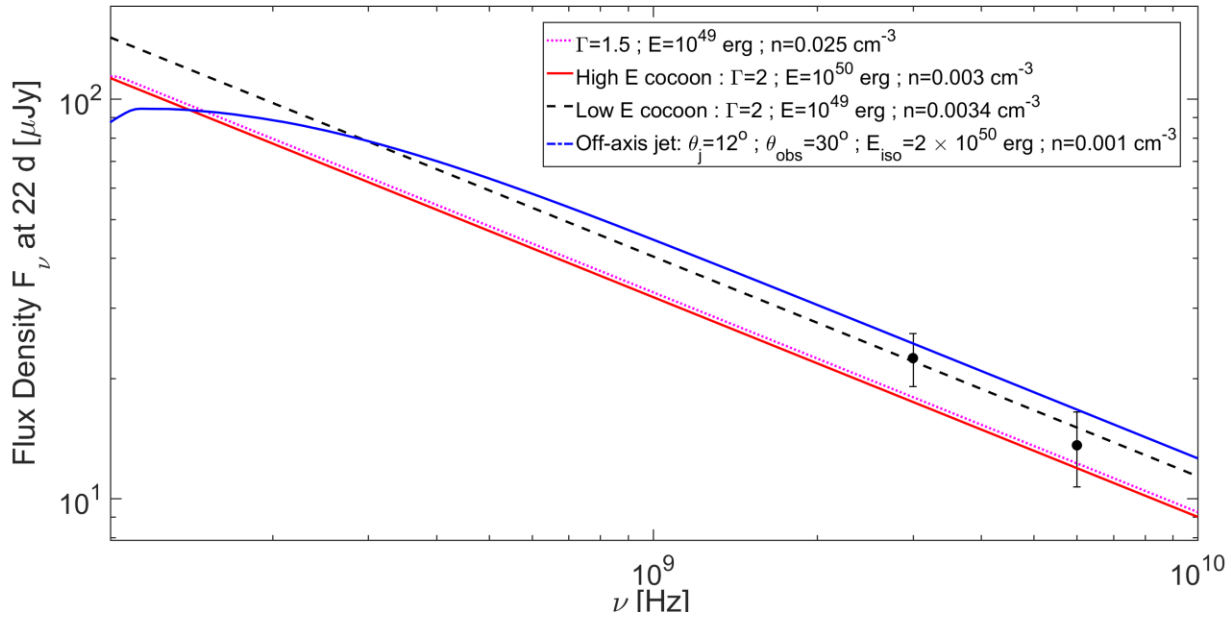

Fig. S4. Radio Spectral Energy Distribution of EM170817. We compare the data taken on September 7 at 6 GHz and September 8 at 3 GHz with the predicted radio spectrum for each of the models shown in Figure 3 at 22 days after the merger (September 8). The predicted spectrum is optically thin between these two frequency bands, which is consistent with the radio data.

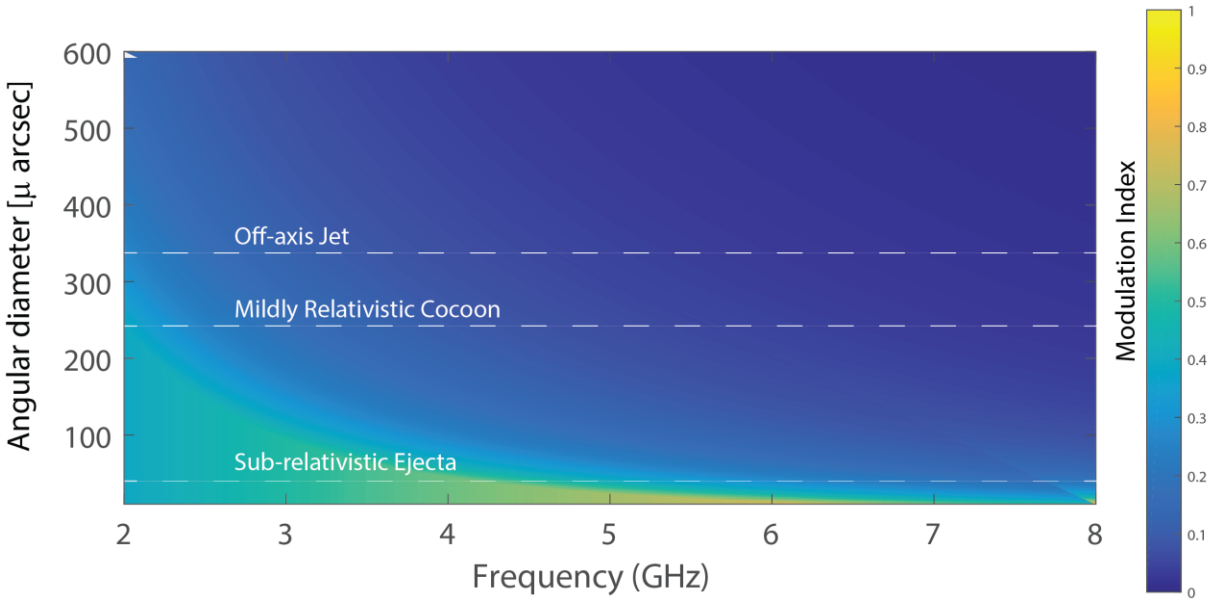

Fig. S5. Predicted refractive scintillation of the radio source for different ejecta models. The expected modulation index (fractional variation) is shown as a function of frequency and source size for refractive scintillation in the direction of EW170817. Horizontal dashed lines show the predicted source size at the time of the first detection (2017, September 2) for the various types of possible ejecta. Scintillation is expected to have had little impact on our observations, except in the unlikely case of radio emission produced by sub-relativistic ejecta, for which ~50% modulations at 3 GHz and 6 GHz would be present on 1 day timescales. This precludes using the light curve variability to establish source size, but does mean that the observed rise in the light curve (Figure 2, 3) is not contaminated by refractive scintillation.

Table S1. Compilation of all data collected as part of this campaign. All upper limits are 3 × RMS except for our VLA observations (excluding VLITE), which are reported as flux at optical location + 2 × RMS.

UT Date	ΔT (d)	Telescope	ν (GHz)	Bandwidth (GHz)	S_ν (mJy)	Reference
Aug 18.21	0.68	ATCA	8.5	2.049	< 0.120	(*54*)
Aug 18.21	0.68	ATCA	10.5	2.049	< 0.150	(*54*)
Aug 18.46	0.93	GMRT	0.61	0.032	< 0.195	(*55*)
Aug 18.92	1.39	VLA	10	3.8	<0.0154†	(*56*)
Aug 18.97	1.44	VLITE/VLA	0.3387	0.034	< 34.8	
Aug 19.95	2.42	VLA	6.2	4	< 0.020	(*57*)
Aug 19.95	2.42	VLA	9.7	4	< 0.017	(*58*)
Aug 19.95	2.42	VLA	15	6	< 0.022	(*59*)
Aug 19.97	2.44	VLITE/VLA	0.3387	0.034	< 28.8	
Aug 20.31	2.78	GMRT	0.4	0.2	< 0.780	(*60*)
Aug 20.46	2.93	GMRT	1.2	0.4	< 0.098	(*60*)
Aug 20.87	3.34	VLA	3	1.6	< 0.032	(*61*)
Aug 20.87	3.34	VLITE/VLA	0.3387	0.034	< 44.7	
Aug 21.23	3.7	ATCA	8.5	2.049	< 0.135	(*62*)
Aug 21.23	3.7	ATCA	10.5	2.049	< 0.099	(*62*)
Aug 22.88	5.35	VLA	6.2	4	< 0.019	(*63*)
Aug 25.90	8.37	VLITE/VLA	0.3387	0.034	< 37.5	
Aug 27.90	10.37	VLA	6.2	4	0.0078 ± 0.0026*	
Aug 28.18	10.65	ATCA	8.5	2.049	< 0.054	(*64*)
Aug 28.18	10.65	ATCA	10.5	2.049	< 0.039	(*64*)
Aug 29.45	11.92	GMRT	0.7	0.4	< 0.123	
Aug 30.98	13.45	VLA	6.2	4	< 0.023	
Aug 30.98	13.45	VLITE/VLA	0.3387	0.034	< 20.4	
Aug 31.46	13.93	GMRT	0.4	0.2	< 0.600	
Sep 01.89	15.37	VLA	6.2	4	< 0.013	
Sep 01.90	15.37	VLITE/VLA	0.3387	0.034	< 11.4	
Sep 02.89	16.36	VLITE/VLA	0.3387	0.034	< 11.7	
Sep 02.95	16.42	VLA	3	2	0.0187 ± 0.0063	(*13*)
Sep 03.01	16.48	VLA	6.2	4	0.0283 ± 0.0054	(*14*)
Sep 03.92	17.39	VLA	3	2	0.0151 ± 0.0039	(*13*)
Sep 03.93	17.4	VLITE/VLA	0.3387	0.034	< 6.9	

Sep 04.86	18.33	VLA	3	2	0.0145 ± 0.0037	
Sep 05.18	18.66	ATCA	7.25	4.098‡	0.025 ± 0.006	(*15*)
Sep 05.52	18.99	GMRT	0.7	0.4	< 0.140	
Sep 05.88	19.35	VLA	6.2	4	0.0159 ± 0.0055	
Sep 07.89	21.36	VLA	6.2	4	0.0136 ± 0.0029	
Sep 07.89	21.36	VLITE/VLA	0.3387	0.034	< 8.1	
Sep 08.89	22.36	VLA	3	2	0.0225 ± 0.0034	
Sep 08.90	22.37	VLITE/VLA	0.3387	0.034	< 6.3	
Sep 09.89	23.36	VLITE/VLA	0.3387	0.034	< 4.8	
Sep 09.89	23.36	VLA	6	4	0.0226 ± 0.0034	
Sep 10.79	24.26	VLA	3	2	0.0256 ± 0.0029	
Sep 10.88	24.35	VLITE/VLA	0.3387	0.034	< 6.6	
Sep 17.75	31.22	VLA	3	2	0.034 ± 0.0036	(*65*)

* Co-added from 22 Aug to Sep 1. Flux density consistent with marginal detection, but no discernible source present in the image.

† Value reflects our own analysis of these public data. A similar limit was reported in (*56*).

‡ 2×2049 MHz bands centred on 5.5 and 9 GHz

References

1. LIGO Scientific Collaboration and Virgo Collaboration, *Phys. Rev. Lett.* **119**, 161101 (2017). 10.1103/PhysRevLett.119.161101

2. A. Goldstein *et al*., *Gamma Ray Coordinates Network Circular 21528* (2017).

3. B. P. Abbott *et al*., Gravitational waves and gamma rays from a binary neutron star merger: GW170817 and GRB 170817A. *Astrophys. J.* 10.3847/2041-8213/aa920c (2017). doi:10.3847/2041-8213/aa920c

4. A. Goldstein *et al*., An ordinary short gamma-ray burst with extraordinary implications: Fermi-GBM detection of GRB 170817A. *Astrophys. J.* 10.3847/2041-8213/aa8f41 (2017). doi:10.3847/2041-8213/aa8f41

5. M. M. Kasliwal, E. Nakar, L. P. Singer, D. L. Kaplan, D. O. Cook, A. Van Sistine, R. M. Lau, C. Fremling, O. Gottlieb, J. E. Jencson, S. M. Adams, U. Feindt, K. Hotokezaka, S. Ghosh, D. A. Perley, P.-C. Yu, T. Piran, J. R. Allison, G. C. Anupama, A. Balasubramanian, K. W. Bannister, J. Bally, J. Barnes, S. Barway, E. Bellm, V. Bhalerao, D. Bhattacharya, N. Blagorodnova, J. S. Bloom, P. R. Brady, C. Cannella, D. Chatterjee, S. B. Cenko, B. E. Cobb, C. Copperwheat, A. Corsi, K. De, D. Dobie, S. W. K. Emery, P. A. Evans, O. D. Fox, D. A. Frail, C. Frohmaier, A. Goobar, G. Hallinan, F. Harrison, G. Helou, T. Hinderer, A. Y. Q. Ho, A. Horesh, W.-H. Ip, R. Itoh, D. Kasen, H. Kim, N. P. M. Kuin, T. Kupfer, C. Lynch, K. Madsen, P. A. Mazzali, A. A. Miller, K. Mooley, T. Murphy, C.-C. Ngeow, D. Nichols, S. Nissanke, P. Nugent, E. O. Ofek, H. Qi, R. M. Quimby, S. Rosswog, F. Rusu, E. M. Sadler, P. Schmidt, J. Sollerman, I. Steele, A. R. Williamson, Y. Xu, L. Yan, Y. Yatsu, C. Zhang, W. Zhao, Illuminating gravitational waves: A concordant picture of photons from a neutron star merger. *Science* 10.1126/science.aap9455 (2017). doi:10.1126/science.aap9455

6. D. Coulter *et al*., *Gamma Ray Coordinates Network Circular 21529* (2017).

7. D. A. Coulter, R. J. Foley, C. D. Kilpatrick, M. R. Drout, A. L. Piro, B. J. Shappee, M. R. Siebert, J. D. Simon, N. Ulloa, D. Kasen, B. F. Madore, A. Murguia-Berthier, Y.-C. Pan, J. X. Prochaska, E. Ramirez-Ruiz, A. Rest, C. Rojas-Bravo, Swope Supernova Survey 2017a (SSS17a), the optical counterpart to a gravitational wave source. *Science* 10.1126/science.aap9811 (2017). doi:10.1126/science.aap9811

8. S. Allam *et al*., *Gamma Ray Coordinates Network Circular 21530* (2017).

9. S. Yang *et al*., *Gamma Ray Coordinates Network Circular 21531* (2017).

10. B. Abbott *et al*., Multi-messenger observations of a binary neutron star merger. *Astrophys. J.* 10.3847/2041-8213/aa91c9 (2017). doi:10.3847/2041-8213/aa91c9

11. P. A. Evans, S. B. Cenko, J. A. Kennea, S. W. K. Emery, N. P. M. Kuin, O. Korobkin, R. T. Wollaeger, C. L. Fryer, K. K. Madsen, F. A. Harrison, Y. Xu, E. Nakar, K. Hotokezaka,

A. Lien, S. Campana, S. R. Oates, E. Troja, A. A. Breeveld, F. E. Marshall, S. D. Barthelmy, A. P. Beardmore, D. N. Burrows, G. Cusumano, A. D'Aì, P. D'Avanzo, V. D'Elia, M. de Pasquale, W. P. Even, C. J. Fontes, K. Forster, J. Garcia, P. Giommi, B. Grefenstette, C. Gronwall, D. H. Hartmann, M. Heida, A. L. Hungerford, M. M. Kasliwal, H. A. Krimm, A. J. Levan, D. Malesani, A. Melandri, H. Miyasaka, J. A. Nousek, P. T. O'Brien, J. P. Osborne, C. Pagani, K. L. Page, D. M. Palmer, M. Perri, S. Pike, J. L. Racusin, S. Rosswog, M. H. Siegel, T. Sakamoto, B. Sbarufatti, G. Tagliaferri, N. R. Tanvir, A. Tohuvavohu, Swift and NuSTAR observations of GW170817: Detection of a blue kilonova. *Science* 10.1126/science.aap9580 (2017). doi:10.1126/science.aap9580

12. See supplementary materials.

13. K. Mooley, G. Hallinan, A. Corsi, *Gamma Ray Coordinates Network Circular 21814* (2017).

14. A. Corsi, G. Hallinan, K. Mooley, *Gamma Ray Coordinates Network Circular 21815* (2017).

15. T. Murphy *et al*., *Gamma Ray Coordinates Network Circular 21842* (2017).

16. S. M. Adams, M. M. Kasliwal, N. Blagorodnova, *Gamma Ray Coordinates Network Circular 21816* (2017).

17. V. Smolčić, M. Novak, M. Bondi, P. Ciliegi, K. P. Mooley, E. Schinnerer, G. Zamorani, F. Navarrete, S. Bourke, A. Karim, E. Vardoulaki, S. Leslie, J. Delhaize, C. L. Carilli, S. T. Myers, N. Baran, I. Delvecchio, O. Miettinen, J. Banfield, M. Baloković, F. Bertoldi, P. Capak, D. A. Frail, G. Hallinan, H. Hao, N. Herrera Ruiz, A. Horesh, O. Ilbert, H. Intema, V. Jelić, H.-R. Klöckner, J. Krpan, S. R. Kulkarni, H. McCracken, C. Laigle, E. Middleberg, E. J. Murphy, M. Sargent, N. Z. Scoville, K. Sheth, The VLA-COSMOS 3 GHz Large Project: Continuum data and source catalog release. *Astron. Astrophys.* **602**, A1 (2017). doi:10.1051/0004-6361/201628704

18. K. P. Mooley, G. Hallinan, S. Bourke, A. Horesh, S. T. Myers, D. A. Frail, S. R. Kulkarni, D. B. Levitan, M. M. Kasliwal, S. B. Cenko, Y. Cao, E. Bellm, R. R. Laher, The Caltech-NRAO Stripe 82 Survey (CNSS) paper. I. The pilot radio transient survey in 50 deg^2. *Astrophys. J.* **818**, 105 (2016). doi:10.3847/0004-637X/818/2/105

19. E. Nakar, T. Piran, Detectable radio flares following gravitational waves from mergers of binary neutron stars. *Nature* **478**, 82–84 (2011). doi:10.1038/nature10365 Medline

20. K. Hotokezaka, T. Piran, Mass ejection from neutron star mergers: Different components and expected radio signals. *Mon. Not. R. Astron. Soc.* **450**, 1430–1440 (2015). doi:10.1093/mnras/stv620

21. K. Hotokezaka, S. Nissanke, G. Hallinan, T. J. W. Lazio, E. Nakar, T. Piran, Radio counterparts of compact binary mergers detectable in gravitational waves: A simulation for an optimized survey. *Astrophys. J.* **831**, 190 (2016). doi:10.3847/0004-637X/831/2/190

22. D. Eichler, M. Livio, T. Piran, D. N. Schramm, Nucleosynthesis, neutrino bursts and γ-rays from coalescing neutron stars. *Nature* **340**, 126–128 (1989). doi:10.1038/340126a0

23. E. Nakar, Short-hard gamma-ray bursts. *Phys. Rep.* **442**, 166–236 (2007). doi:10.1016/j.physrep.2007.02.005

24. J. Granot, A. Panaitescu, P. Kumar, S. E. Woosley, Off-axis afterglow emission from jetted gamma-ray bursts. *Astrophys. J.* **570**, L61–L64 (2002). doi:10.1086/340991

25. R. Sari, T. Piran, R. Narayan, Spectra and light curves of gamma-ray burst afterglows. *Astrophys. J.* **497**, L17–L20 (1998). doi:10.1086/311269

26. E. Berger, Short-duration gamma-ray bursts. *Annu. Rev. Astron. Astrophys.* **52**, 43–105 (2014). doi:10.1146/annurev-astro-081913-035926

27. P. Serra, T. Oosterloo, R. Morganti, K. Alatalo, L. Blitz, M. Bois, F. Bournaud, M. Bureau, M. Cappellari, A. F. Crocker, R. L. Davies, T. A. Davis, P. T. de Zeeuw, P.-A. Duc, E. Emsellem, S. Khochfar, D. Krajnović, H. Kuntschner, P.-Y. Lablanche, R. M. McDermid, T. Naab, M. Sarzi, N. Scott, S. C. Trager, A.-M. Weijmans, L. M. Young, The ATLAS3D project - XIII. Mass and morphology of H I in early-type galaxies as a function of environment. *Mon. Not. R. Astron. Soc.* **422**, 1835–1862 (2012). doi:10.1111/j.1365-2966.2012.20219.x

28. O. Gottlieb, E. Nakar, T. Piran, The cocoon emission - an electromagnetic counterpart to gravitational waves from neutron star mergers. arXiv:1705.10797 (2017).

29. E. Troja *et al.*, *Gamma Ray Coordinates Network Circular 21765* (2017).

30. E. Troja *et al.*, *Nature* 10.1038/nature24290 (2017). doi:10.1038/nature24290

31. X.-G. Wang, B. Zhang, E.-W. Liang, H. Gao, L. Li, C.-M. Deng, S.-M. Qin, Q.-W. Tang, D. A. Kann, F. Ryde, P. Kumar, How bad or good are the external forward shock afterglow models of gamma-ray bursts? *Astrophys. J. Suppl. Ser.* **219**, 9 (2015). doi:10.1088/0067-0049/219/1/9

32. S. R. Kulkarni, D. A. Frail, M. H. Wieringa, R. D. Ekers, E. M. Sadler, R. M. Wark, J. L. Higdon, E. S. Phinney, J. S. Bloom, Radio emission from the unusual supernova 1998bw and its association with the γ-ray burst of 25 April 1998. *Nature* **395**, 663–669 (1998). doi:10.1038/27139

33. G. B. Taylor, D. A. Frail, E. Berger, S. R. Kulkarni, The angular size and proper motion of the afterglow of GRB 030329. *Astrophys. J.* **609**, L1–L4 (2004). doi:10.1086/422554

34. M. A. Walker, Interstellar scintillation of compact extragalactic radio sources. *Mon. Not. R. Astron. Soc.* **294**, 307–311 (1998). doi:10.1111/j.1365-8711.1998.01238.x

35. J. M. Cordes, T. J. W. Lazio, NE2001.I. A new model for the galactic distribution of free electrons and its fluctuations. arXiv:astro-ph/0207156 (2002).

36. R. A. Perley, C. J. Chandler, B. J. Butler, J. M. Wrobel, The Expanded Very Large Array: A new telescope for new science. *Astrophys. J.* **739**, L1 (2011). doi:10.1088/2041-8205/739/1/L1

37. J. P. McMullin *et al*., *ADASS XVI ASP Conf. Ser.* **376**, 127 (2007).

38. J. A. Högbom, Aperture synthesis with a non-regular distribution of interferometer baselines. *Astron. Astrophys. Suppl. Ser.* **15**, 417 (1974).

39. R. J. Sault, P. J. Teuben, M. C. H. Wright, *ADASS IV Conf. Ser.* **77**, 433 (1995).

40. M. C. Shepherd, *ADASS VI ASP Conf. Ser.* **125**, 77 (1997).

41. J. Roy, Y. Gupta, U.-L. Pen, J. B. Peterson, S. Kudale, J. Kodilkar, A real-time software backend for the GMRT. *Exp. Astron.* **28**, 25–60 (2010). doi:10.1007/s10686-010-9187-0

42. H. T. Intema, S. van der Tol, W. D. Cotton, A. S. Cohen, I. M. van Bemmel, H. J. A. Röttgering, Ionospheric calibration of low frequency radio interferometric observations using the peeling scheme. *Astron. Astrophys.* **501**, 1185–1205 (2009). doi:10.1051/0004-6361/200811094

43. S. H. Reddy, S. Kudale, U. Gokhale, I. Halagalli, N. Raskar, K. De, S. Gnanaraj, B. A. Kumar, Y. Gupta, A wideband digital back-end for the upgraded GMRT. *J. Astron. Instrum.* **6**, 1641011 (2017). doi:10.1142/S2251171716410117

44. T. E. Clarke, N. E. Kassim, W. Brisken, J. Helmboldt, W. Peters, P. S. Ray, E. Polisensky, S. Giacintucci, Commensal low frequency observing on the NRAO VLA: VLITE status and future plans. *Proc. SPIE* **9906**, 99065B (2016). doi:10.1117/12.2233036

45. E. W. Greisen, FITS: A remarkable achievement in information exchange. In *Information Handling in Astronomy—Historical Vistas*, A. Heck, Ed. (Springer, 2003), pp. 71–87.

46. W. D. Cotton, Obit: A development environment for astronomical algorithms. *Publ. Astron. Soc. Pac.* **120**, 439–448 (2008). doi:10.1086/586754

47. R. M. Prestage, K. T. Constantikes, T. R. Hunter, L. J. King, R. J. Lacasse, F. J. Lockman, R. D. Norrod, The Green Bank Telescope. *Proc. IEEE* **97**, 1382–1390 (2009). doi:10.1109/JPROC.2009.2015467

48. G. de Vaucouleurs, A. de Vaucouleurs, H. G. Corwin, R. J. Buta, P. Fouque, G. Paturel, *Third Reference Catalogue of Bright Galaxies, Volumes I to III* (Springer, 1991).

49. A. Soderberg, E. Nakar, E. Berger, S. R. Kulkarni, Late-time radio observations of 68 type Ibc supernovae: Strong constraints on off-axis gamma-ray bursts. *Astrophys. J.* **638**, 930–937 (2006). doi:10.1086/499121

50. H. van Eerten, A. van der Horst, A. MacFadyen, Gamma-ray burst afterglow broadband fitting based directly on hydrodynamics simulations. *Astrophys. J.* **749**, 44 (2012). doi:10.1088/0004-637X/749/1/44

51. Y. Oren, E. Nakar, T. Piran, The apparent size of gamma-ray burst afterglows as a test of the fireball model. *Mon. Not. R. Astron. Soc.* **353**, 35 (2004). doi:10.1111/j.1365-2966.2004.08247.x

52. D. G. Barnes, L. Staveley-Smith, W. J. G. de Blok, T. Oosterloo, I. M. Stewart, A. E. Wright, G. D. Banks, R. Bhathal, P. J. Boyce, M. R. Calabretta, M. J. Disney, M. J. Drinkwater, R. D. Ekers, K. C. Freeman, B. K. Gibson, A. J. Green, R. F. Haynes, P. Te Lintel Hekkert, P. A. Henning, H. Jerjen, S. Juraszek, M. J. Kesteven, V. A. Kilborn, P. M. Knezek, B. Koribalski, R. C. Kraan-Korteweg, D. F. Malin, M. Marquarding, R. F. Minchin, J. R. Mould, R. M. Price, M. E. Putman, S. D. Ryder, E. M. Sadler, A. Schroder, F. Stootman, R. L. Webster, W. E. Wilson, T. Ye, The H I Parkes All Sky Survey: Southern observations, calibration and robust imaging. *Mon. Not. R. Astron. Soc.* **322**, 486–498 (2001). doi:10.1046/j.1365-8711.2001.04102.x

53. R. C. Kennicutt Jr., The global Schmidt law in star-forming galaxies. *Astrophys. J.* **498**, 541–552 (1998). doi:10.1086/305588

54. D. Kaplan *et al.*, *Gamma Ray Coordinates Network Circular 21574* (2017).

55. K. De *et al.*, *Gamma Ray Coordinates Network Circular 21603* (2017).

56. K. Alexander, W. Fong, E. Berger, *Gamma Ray Coordinates Network Circular 21589* (2017).

57. A. Corsi, M. M. Kasliwal, *Gamma Ray Coordinates Network Circular 21614* (2017).

58. A. Corsi, M. M. Kasliwal, *Gamma Ray Coordinates Network Circular 21613* (2017).

59. A. Corsi, M. M. Kasliwal, *Gamma Ray Coordinates Network Circular 21636* (2017).

60. K. De *et al.*, *Gamma Ray Coordinates Network Circular 21708* (2017).

61. K. P. Mooley, G. Hallinan, *Gamma Ray Coordinates Network Circular 21650* (2017).

62. C. Lynch *et al.*, *Gamma Ray Coordinates Network Circular 21670* (2017).

63. A. Corsi, M. M. Kasliwal, D. Frail, N. T. Palliyaguru, *Gamma Ray Coordinates Network Circular 21664* (2017).

64. C. Lynch *et al.*, *Gamma Ray Coordinates Network Circular 21740* (2017).

65. G. Hallinan *et al.*, *Gamma Ray Coordinates Network Circular 21929* (2017).